Truong X. Tran 🆔

COLLECTIONS

ⓔⓟ   This paper was selected as an Editor's Pick

View Online   Export Citation   CrossMark

ARTICLES YOU MAY BE INTERESTED IN

Topological analysis of SARS CoV-2 main protease
Chaos: An Interdisciplinary Journal of Nonlinear Science **30**, 061102 (2020); https://doi.org/10.1063/5.0013029

Ergodicity, mixing, and recurrence in the three rotor problem
Chaos: An Interdisciplinary Journal of Nonlinear Science **30**, 043112 (2020); https://doi.org/10.1063/1.5141067

Nonlinear dynamics of continuous-time random walks in inhomogeneous medium
Chaos: An Interdisciplinary Journal of Nonlinear Science **30**, 063135 (2020); https://doi.org/10.1063/5.0002370

Jackiw–Rebbi states and trivial states in interfaced binary waveguide arrays with cubic–quintic nonlinearity ⓔ

Truong X. Tran[a] 🆔

AFFILIATIONS

Department of Physics, Le Quy Don Technical University, 236 Hoang Quoc Viet str., 10000 Hanoi, Vietnam

[a]**Author to whom correspondence should be addressed:** tranxtr@gmail.com

ABSTRACT

We systematically investigate two types of localized states—one is the optical analog of the quantum relativistic Jackiw–Rebbi states and the other is the trivial localized state—in interfaced binary waveguide arrays in the presence of cubic–quintic nonlinearity. By using the shooting method, we can exactly calculate the profiles of these nonlinear localized states. Like in the case with Kerr nonlinearity, we demonstrate that these localized states with cubic–quintic nonlinearity also have an extraordinary property, which completely differs from *many* well-known nonlinear localized structures in other media. Specifically, both the peak amplitude and transverse dimension of these nonlinear localized states can increase at the same time. Apart from that, we show that high values of the saturation nonlinearity parameter can help to generate and stabilize the intense localized states during propagation, especially in the case with a negative coefficient for the cubic nonlinearity term.

Published under license by AIP Publishing. https://doi.org/10.1063/5.0004073

The optical analog of the topological quantum relativistic Jackiw–Rebbi (JR) state and the trivial localized state has been found earlier in interfaced binary waveguide arrays (BWAs) both in the linear regime and in the case of Kerr nonlinearity. Due to their topological nature, JR states in BWAs have been demonstrated to be extremely robust under the influence of strong disturbances. This feature can be useful in the design of all-optical circuits. In this work, we investigate the JR states and trivial localized states in the regime of cubic–quintic nonlinearity in interfaced BWAs. We use the shooting method to calculate the exact profiles of these localized states and study their properties. We demonstrate that large values of the saturation nonlinearity parameter in the regime of cubic–quintic nonlinearity can be exploited to stabilize these intense localized states.

I. INTRODUCTION

Waveguide arrays (WAs) present interesting platforms to investigate many fundamental photonic phenomena in classical physics such as discrete diffraction,[1,2] discrete solitons,[1,3–5] and diffractive resonant radiation.[6] These platforms also can mimic fundamental effects in nonrelativistic quantum mechanics emerging from the Schrödinger equation.[7,8] Moreover, binary waveguide arrays (BWAs) can be very useful in studying relativistic quantum mechanics phenomena rooted in the Dirac equations. Indeed, in the last decade, many relativistic quantum mechanics phenomena, e.g., *Zitterbewegung,*[9] the Klein paradox,[10] and Dirac solitons[11–16] have been thoroughly analyzed in BWAs.

In 2017, the exact *linear* localized solutions for the optical analog of *Jackiw–Rebbi* (JR) states and trivial states were found in Ref. 17 at the interface of two BWAs. The JR states are quantum relativistic structures and quite well known in quantum field theory.[18] Thanks to the JR states, the phenomenon of charge fractionalization (which is crucial in the discovery of the fractional quantum Hall effect[19]) has been predicted. The so-called zero-energy solution of JR states possesses the topological nature, which is fundamental in topological insulators.[20] Recently, topological photonics has attracted a great amount of interest in designing robust optical circuits.[21–24] In 2019, the extreme robustness of the JR states in interfaced BWAs under the influence of strong disturbances was demonstrated.[25] Different scenarios of interactions between JR states and Dirac solitons have been analyzed in BWAs in Ref. 26.

As mentioned above, JR states and trivial states in BWAs have been analytically and numerically investigated only in the *linear*

regime in Ref. 17. These localized solutions in the regime of Kerr nonlinearity have been systematically investigated later in Ref. 27 both for self-focusing and self-defocusing nonlinearity by using the shooting method.[28] This model with Kerr nonlinearity is the simplest one for studying third-order nonlinear effects in optics. However, if the optical signals are intense enough, one needs to take into account the fifth and even higher-order terms for nonlinearity. The resulting equation in that case is often called the cubic–quintic nonlinear Schrödinger equation (NLS) because it contains terms accounting for both the third and fifth powers of the signal amplitude. In fiber optics, this cubic–quintic NLS for a *single* fiber has been well studied.[29] In one-dimensional[30–33] and higher-dimensional[34] WAs consisting of just one type of waveguide, solitons and other localized structures rooted in the system of cubic–quintic NLS have also attracted a great amount of attention.

In this work, we study the JR states and trivial states in interfaced BWAs with cubic–quintic nonlinearity. The remainder of this paper is organized as follows: in Sec. II, as a starting point, we re-introduce the exact solutions for linear JR states and trivial states, which have already been obtained in Ref. 17. Then, in Sec. III, we investigate the profiles of these two types of localized states with cubic–quintic nonlinearity. In Sec. IV, we focus on the detunings of these nonlinear localized states. Finally, in Sec. V, we summarize our results and finish with concluding remarks.

II. GOVERNING EQUATIONS AND LINEAR SOLUTIONS OF JACKIW–REBBI STATES AND TRIVIAL STATES

As a starting point, in this section, we present the governing equations in interfaced BWAs with cubic–quintic nonlinearity and the exact solutions of JR states and trivial states, which have

been found earlier in the *linear* regime in Ref. 17. This is necessary because some results of linear JR and trivial solutions, in particular, their detunings, will be needed later for discussion of nonlinear localized states with cubic–quintic nonlinearity.

The light beam propagation in BWAs with cubic–quintic nonlinearity can be governed by the following dimensionless discrete coupled-mode equations (CMEs):

$$i\frac{da_n}{dz} + \kappa[a_{n+1} + a_{n-1}] - (-1)^n \sigma a_n + \gamma(1 - b_s|a_n|^2)|a_n|^2 a_n = 0.$$
(1)

In Eq. (1), a_n represents the electric field amplitude in the nth waveguide, z is the longitudinal spatial variable, 2σ is the propagation mismatch, κ is the coupling coefficient between two adjacent waveguides of the array, γ is the nonlinear coefficient of the cubic terms of waveguides, and b_s is the saturation parameter governing the power level at which the nonlinearity saturation effect starts to take place. For many materials, $b_s|a_n|^2 \ll 1$ in most practical situations. However, this nonlinear term can become noticeable when the peak intensity of the light signal is around $1\,\mathrm{GW/cm^2}$ in the case of silica.[35] Note that the cubic–quintic nonlinearity is also known as competing nonlinearities, and b_s is always positive for most of optical media, e.g., semiconductor waveguides, organic polymers, and semiconductor-doped glasses.[4] It is also worth mentioning that the cubic–quintic nonlinearity is a special case of a more general kind of nonlinearity known as saturable nonlinearity, which exists in many nonlinear media [see Eq. (7.4.1) in Ref. 4].

In order to generate JR states, one needs to use two BWAs, which are close to each other as schematically shown in Fig. 1(a). Note that if $n < 0$ (for the left-hand side BWA), then σ takes the
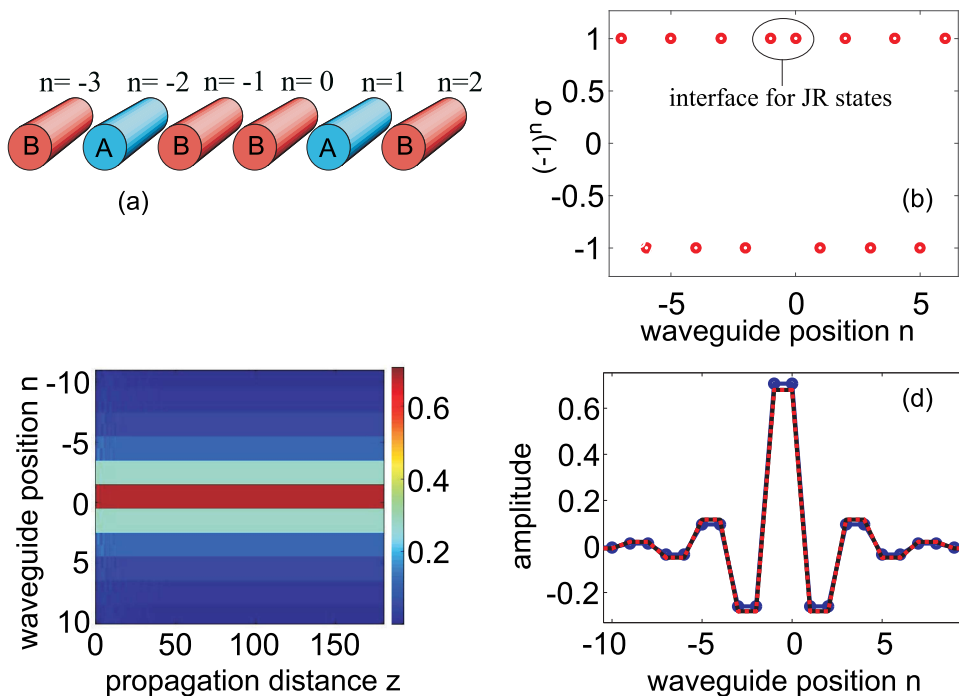
FIG. 1. (a) The system of interfaced BWAs created by two BWAs put close to each other. (b) The value distribution of the array $(-1)^n\sigma$, which can support the discrete JR states. (c) Propagation of a linear JR state in interfaced BWAs where Eq. (3) is used as an input condition. (d) Curves showing the amplitudes of the JR state at input (solid blue with round markers) and output (solid black), which is hidden behind the dotted red curve representing the discrete JR state in the form of Eq. (4). Parameters are $-\sigma_1 = \sigma_2 = 1$, $\kappa = 1$, and $\gamma = 0$. Figures 1(a), 1(c), and 1(d) are reproduced from Fig. 1 in Ref. 17.

constant value σ_1; whereas if $n \geq 0$ (the right-hand side BWA), then σ takes the constant value σ_2.

As in Refs. 9 and 36, by setting $\Psi_1(n) = (-1)^n a_{2n}$, $\Psi_2(n) = i(-1)^n a_{2n-1}$, and using the continuous transverse coordinate $\xi \leftrightarrow n$, one can get the following Dirac equation in the regime of cubic–quintic nonlinearity for the two-component spinor $\Psi(\xi, z) = (\Psi_1, \Psi_2)^T$:

$$i\partial_z \Psi = -i\kappa \hat{\sigma}_x \partial_\xi \Psi + \sigma \hat{\sigma}_z \Psi - \gamma G + \gamma b_s F, \qquad (2)$$

where the cubic nonlinearity is taken into account via the term $G \equiv (|\Psi_1|^2 \Psi_1, |\Psi_2|^2 \Psi_2)^T$; the quintic nonlinearity is taken into account via the term $F \equiv (|\Psi_1|^4 \Psi_1, |\Psi_2|^4 \Psi_2)^T$; $\hat{\sigma}_x$ and $\hat{\sigma}_z$ are the usual Pauli matrices. In the case of just Kerr nonlinearity, the resulting equation will be simplified as Eq. (7) in Ref. 11 without the quintic term.

In the *linear* regime, if $\sigma_1 < 0$ and $\sigma_2 > 0$, then the following exact continuous JR solutions of Eq. (2) have been obtained analytically earlier in Ref. 17:

$$\Psi(\xi) = \sqrt{\frac{|\sigma_1 \sigma_2|}{\kappa(|\sigma_1| + |\sigma_2|)}} \begin{pmatrix} 1 \\ i \end{pmatrix} e^{-|\sigma(\xi)\xi|/\kappa}. \qquad (3)$$

Note that the continuous solution in the form of Eq. (3) is the exact *linear* solution to the continuous equation (2) when $\gamma = 0$, but it is only an approximate linear solution to the discrete equation (1). It is obvious that this approximation gets better when the beam width increases. Note also that $\sigma(\xi) = \sigma_1$ if $\xi < 0$ and $\sigma(\xi) = \sigma_2$ if $\xi \geq 0$.

As already pointed out in Ref. 17, when the function $\sigma(\xi)$ has the form of the hyperbolic tangent function, Jackiw and Rebbi have found topological localized JR states for the Dirac equation (2)—which are also known as the zero-modes, zero-energy states.[18,37,38] In our case, the function $\sigma(\xi)$ has the form of a step-like function, which brings us to the localized JR solution (3), and it corresponds to the limit when the scale kink of the JR model has an infinite steepness. What is important here is the difference in sign of the function $\sigma(\xi)$, but not the smoothness of the transition.

If $|\sigma_1| = |\sigma_2| = \sigma_0$, as found earlier in Ref. 17, we can obtain exact localized solutions to Eq. (1) in the linear regime in the two cases as follows:

If $-\sigma_1 = \sigma_2 = \sigma_0 > 0$, then we get the discrete JR state,[17]

$$a_n(z) = b_n e^{i\delta_1 z}, \qquad (4)$$

where the detuning $\delta_1 \equiv \kappa - \sqrt{\sigma_0^2 + \kappa^2}$, b_n is real and always independent of z, and $b_{2n-1} = b_{2n}$. If $n \geq 0$, we have $b_{2n}/b_{2n+1} = \alpha \equiv -[\sigma_0/\kappa + \sqrt{1 + \sigma_0^2/\kappa^2}]$; whereas if $n < 0$, we have $b_{2n+1}/b_{2n} = \alpha$. For hosting these discrete JR states, two adjacent waveguides at the interface must have positive values for $(-1)^n\sigma$ [see Fig. 1(b) at the central region for more details]. We want to stress that from this discrete solution b_n, one can easily construct the component $\Psi_1(n)$, which has the *same* sign for all n (obviously, after dropping the common factor $e^{i\delta_1 z}$). This is also true for $\Psi_2(n)$. Therefore, the derivative $\partial_\xi \Psi$ in Eq. (2) mathematically makes sense in this case, and the discrete solution (4) can be claimed as the approximate discrete JR solution to the continuous Dirac equation (2).

However, if $\sigma_1 = -\sigma_2 = \sigma_0 > 0$, we get the following trivial localized state:[17]

$$a_n(z) = b_n e^{i\delta_2 z}, \qquad (5)$$

where the detuning $\delta_2 \equiv \kappa + \sqrt{\sigma_0^2 + \kappa^2}$, b_n is also real and independent of z, and $b_{2n-1} = b_{2n}$. If $n \geq 0$, we get $b_{2n}/b_{2n+1} = -\alpha$; whereas if $n < 0$, we get $b_{2n+1}/b_{2n} = -\alpha$. For hosting these trivial states, two adjacent waveguides at the interface must have negative values for $(-1)^n\sigma$. Here, we want to emphasize that from this discrete solution b_n, one can easily construct the component $\Psi_1(n)$, which has *opposite* signs for neighboring values of n (obviously, after dropping the common factor $e^{i\delta_1 z}$); i.e., $\Psi_1(n)\Psi_1(n+1) \leq 0$ for all n. This is also true for $\Psi_2(n)$. Therefore, the derivative $\partial_\xi \Psi$ in Eq. (2) mathematically does not make sense in this case, and the discrete solution (5), unlike the solution (4), cannot be claimed as the approximate JR solution to the continuous Dirac equation (2). That is the reason why we here explicitly call Eq. (5) a trivial localized solution to Eq. (1).

There is one principal difference between JR (topological) states and trivial (non-topological) states: JR states are gap states, whereas trivial states are non-gap states. Indeed, if the system is just a periodic BWA without any defect, i.e., without the interface, then in the linear regime, by making the following ansatz for a plane wave

$$a_n(Q) \sim \exp[i(Qn - \omega z)], \qquad (6)$$

one can get the dispersion relations from Eq. (1) as follows:[39]

$$\omega_\pm(Q) = \pm\sqrt{\sigma_0^2 + 4\kappa^2 \cos^2 Q}. \qquad (7)$$

As clearly shown from Eq. (7), two bands ω_+ and ω_+ are separated by a gap from $-\sigma_0$ to σ_0. Moreover, the detuning δ_1 of the JR states defined below solution (4) is inside this gap (because the coupling coefficient κ is always positive), i.e., $-\sigma_0 < \delta_1 < \sigma_0$, whereas the detuning δ_2 of the trivial states defined below solution (5) is outside this gap, i.e., $\sigma_0 < \delta_2$. Note also that the Dirac solitons found in Ref. 11 in a periodic BWA have also been shown to be gap solitons (see Ref. 15).

In Fig. 1(b), we show the value distribution of the array $(-1)^n\sigma$ for the interfaced BWAs, which can support the discrete JR states. In Fig. 1(c), we show the propagation of a JR state in the linear regime where the continuous JR solution in the form of Eq. (3) is used as the initial condition for numerically solving the discrete equation (1). In Fig. 1(d), we plot the input (the solid blue curve having round markers), which is constructed by using the continuous JR solution (3), and output beam amplitudes (the solid black curve) taken from Fig. 1(c). The dotted red curve in Fig. 1(d) represents the exact discrete JR solution (4) to Eq. (1). However, in Fig. 1(d), one cannot clearly see the output solid black curve because it is totally hidden behind the dotted red curve. This fact demonstrates that the continuous JR solution (3) is an excellent approximate solution for the discrete Eq. (1). Similarly, the discrete JR solution (4) is also an excellent approximate solution for the continuous Dirac equation (2). In other words, this fact confirms that the discrete solution (4) can be claimed as a true JR state solution.

With the aim to provide real physical values for this JR state, one can get typical parameters in WAs made of AlGaAs,[40] where the

coupling coefficient in physical units is $K = 1240 \, \text{m}^{-1}$ and the nonlinear coefficient is $\Gamma = 6.5 \, \text{m}^{-1}\text{W}^{-1}$. In this case, the power scale will be $P_0 = K/\Gamma = 190.8 \, \text{W}$; therefore, the peak power shown in Fig. 1(d) will be around 94 W, and the length scale in the propagation direction will be $z_0 = 1/K = 0.8 \, \text{mm}$. For conversion from the calculated dimensionless units into the physical units and vice versa in BWAs, one can refer to Ref. 25 for more details.

III. LOCALIZED JACKIW–REBBI STATES AND TRIVIAL STATES WITH CUBIC–QUINTIC NONLINEARITY

We are now able to investigate the localized solutions in the case of cubic–quintic nonlinearity. To be more concrete, we will solve the discrete equation (1) in the full form. Like in the case of Kerr nonlinearity investigated in Ref. 27, the nonlinear localized solutions will be found by using the following form:

$$a_n(z) = b_n e^{i\delta z}, \tag{8}$$

where the nonlinear amplitude b_n is real, independent of z, and still unknown for now. For each nonlinear localized state, the detuning δ is the eigenvalue and needs to be looked into further. Obviously, in the linear case, the detuning δ acquires the constant value either δ_1 for the discrete JR state or δ_2 for the trivial localized state. By using the ansatz (8) for Eq. (1), we obtain a system of algebraic cubic–quintic equations as follows:

$$-\delta b_n = -\kappa[b_{n+1} + b_{n-1}] + (-1)^n \sigma b_n - \gamma(1 - b_s|b_n|^2)|b_n|^2 b_n. \tag{9}$$

Now, we can use certain numerical methods, such as the shooting method to numerically solve Eq. (9) for obtaining the nonlinear localized solutions with cubic–quintic nonlinearity and their detuning values. This shooting method[28] has been described in detail in Ref. 27 to find localized solutions with Kerr nonlinearity. This method can also be successfully used for any other kind of nonlinearity, including the cubic–quintic one as in this work. The essence of this method is that for each fixed value of the peak amplitude $b_0 = b_{-1}$, one can find the eigenvalue (if it exists) of the detuning δ such that the tails of the nonlinear localized states will vanish when $n \to \pm\infty$; i.e., $b_n \to 0$ when n is big enough.[27]

In Fig. 2(a), we present the amplitude profile $|b_n|$ of a JR state when $\gamma = 1$. In Fig. 2(a), the red curve having round markers is when the saturation nonlinearity parameter $b_s = 0.1$ and the peak amplitude $b_0 = 1$ (the eigenvalue of the detuning is found to be $\delta \simeq -0.6682\delta_1$), the dashed blue curve is when $b_s = 0.4$, $b_0 = 1$ (with $\delta \simeq -0.1360\delta_1$), and the dotted green curve is when $b_s = 0.4$, $b_0 = 0.8$ (with $\delta \simeq 0.1183\delta_1$). In Fig. 2(b), we show the evolution of the nonlinear localized JR state in the (n, z)-plane by solving Eq. (1) where the red curve having round markers in Fig. 2(a) serves as the initial condition, i.e., when $\gamma = 1$, $b_0 = b_{-1} = 1.0$, and $b_s = 0.1$. It is clearly shown in Fig. 2(b) that this nonlinear JR state can perfectly conserve its profile during propagation for a very long distance.

In Fig. 2(c), we plot the amplitude profiles $|b_n|$ of JR states with $\gamma = -1$ and peak amplitude $b_0 = b_{-1} = 0.8$ for two values of the saturation parameter b_s: the red curve having round markers is when $b_s = 0.1$ (with $\delta \simeq 2.095\delta_1$), and the dashed blue curve is when $b_s = 0.4$ (with $\delta \simeq 1.88\delta_1$). The latter curve is served as initial conditions for solving Eq. (1), and the evolution in the (n, z)-plane of

this JR state is illustrated in Fig. 2(d). In Fig. 2(e), we show the evolution of the JR state when $\gamma = -1$, $b_0 = b_{-1} = 0.5$, and $b_s = 0.1$ (with $\delta \simeq 1.4428\delta_1$). Meanwhile, in Fig. 2(f), we show the evolution of the JR state with all parameters as in Fig. 2(e) except for the input peak amplitude $b_0 = b_{-1} = 0.8$ (with $\delta \simeq 2.095\delta_1$) in Fig. 2(f) instead of the value $b_0 = b_{-1} = 0.5$ in Fig. 2(e). In Fig. 2, we use all other parameters as follows: $\sigma_1 = -1$, $\sigma_2 = 1$, and the coupling coefficient $\kappa = 1$.

In Fig. 3, we show the trivial localized states in the regime of cubic–quintic nonlinearity. In Fig. 3(a), we plot the amplitude profiles b_n of the trivial state having the peak amplitude $b_0 = b_{-1} = 1.0$ in the regime when $\gamma = 1$ with two values of the saturation parameter b_s: the red curve with round markers is obtained when $b_s = 0.1$ and $\delta \simeq 1.3172\delta_2$, whereas the dashed blue curve is obtained when $b_s = 0.4$ and $\delta \simeq 1.2071\delta_2$. These trivial states are also very robust and can propagate without any distortion of their shapes for quite a long distance. Indeed, as an example, in Fig. 3(b), we demonstrate the evolution in the (n, z)-plane of the trivial state with the input condition taken from the dashed blue curve in Fig. 3(a). Similarly, in Fig. 3(c), we plot the amplitude profiles b_n of the trivial states when $\gamma = -1$: the red curve with round markers is obtained when $b_s = 0.1$, $b_0 = 0.4$ (with $\delta \simeq 0.9527\delta_2$); the dashed blue curve is obtained when $b_s = 0.4$, $b_0 = 0.4$ (with $\delta \simeq 0.9548\delta_2$), whereas the dotted green curve is obtained when $b_s = 0.4$, $b_0 = 0.3$ (with $\delta \simeq 0.9735\delta_2$). The dashed blue curve in Fig. 3(c) is used as input conditions for investigating the trivial state in the (n, z)-plane shown in Fig. 3(d).

We can see that there are some common properties between the profiles of localized states with cubic–quintic nonlinearity shown in Figs. 2 and 3 of this work and those with Kerr nonlinearity reported in Ref. 27. First, if γ is positive, then all the profiles of nonlinear localized states in interfaced BWAs decrease in a monotonic manner from the center to each tail, whereas this is not the case if γ is negative. Second, if we fix all parameters of nonlinear states except for the sign of γ (and the eigenvalue δ, of course), then the profiles of nonlinear states with positive γ are more localized in the transverse direction than those with negative γ. Apart from these common points, the quintic term with the saturation parameter b_s leads to some new interesting features. First and foremost, b_s can help to stabilize nonlinear states and suppress the noise during propagation, especially in the regime of self-defocusing nonlinearity for the cubic term (i.e., when $\gamma = -1$). Indeed, in Figs. 2(d) and 2(f), as an example, we show the propagation of discrete JR states with all the same parameters except for the only difference that the saturation parameter $b_s = 0.4$ in Fig. 2(d), but $b_s = 0.1$ in Fig. 2(f). The discrete JR state with greater b_s shown in Fig. 2(d) is perfectly stable during propagation. Meanwhile, the discrete JR state with smaller b_s shown in Fig. 2(f) is only stable at the beginning up to the distance $z \simeq 300$; after that, the noise grows up and totally destroys the discrete JR state at the output. Therefore, one can say that discrete media such as BWAs with a larger saturation parameter b_s are more favorable to support the stable propagation of nonlinear localized states. Note that, in bulk media, the saturable nonlinearity is also well known for being able to arrest the pulse collapse and helping to form stable light bullets (a spatiotemporal soliton).[4] Note also that the saturation parameter is more crucial in stabilizing localized states with the negative γ. In the case of positive γ, our simulations show that
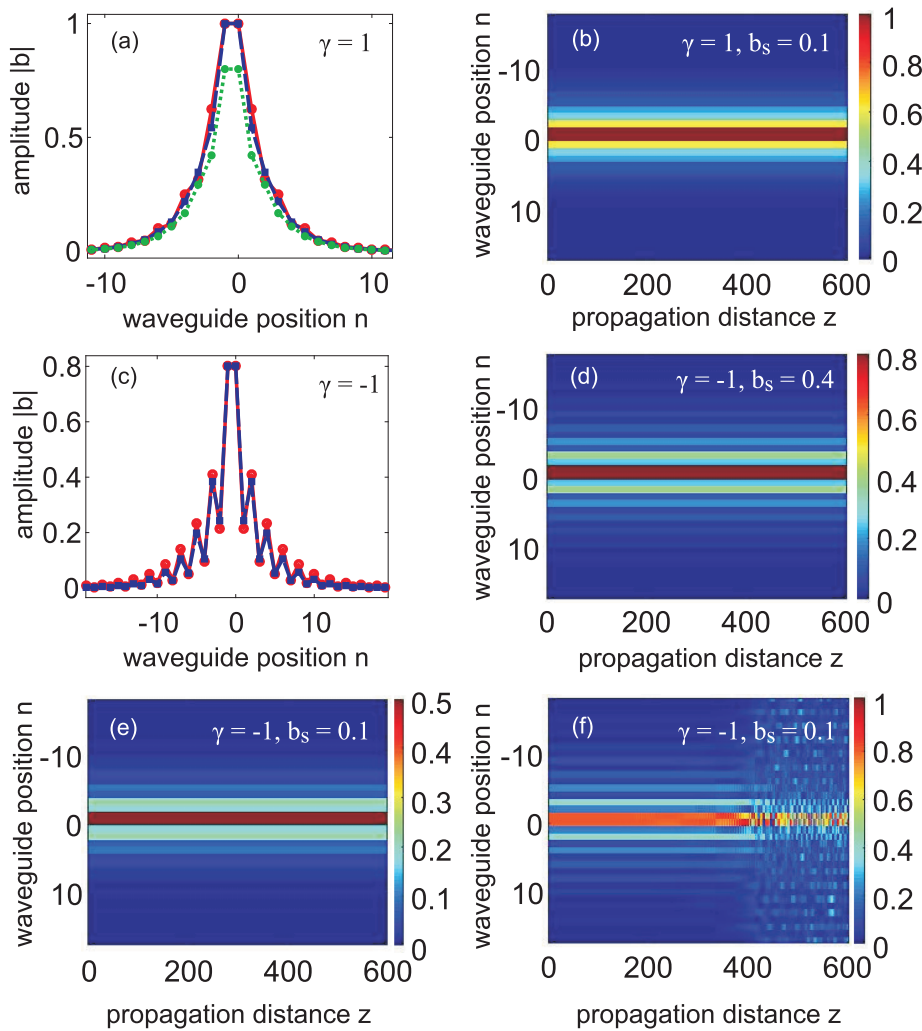
FIG. 2. Localized discrete JR states in interfaced BWAs with cubic–quintic nonlinearity. (a) Amplitude profile $|b_n|$ when $\gamma = 1$: the red curve having round markers is when $b_s = 0.1$ and $b_0 = 1$, the dashed blue curve is when $b_s = 0.4$ and $b_0 = 1$, whereas the dotted green curve is when $b_s = 0.4$ and $b_0 = 0.8$. (b) Evolution of the nonlinear JR state with the input condition taken from the red curve having round markers in (a). (c) Amplitude profile $|b_n|$ when $\gamma = -1$ and $b_0 = 0.8$: the red curve having round markers is when $b_s = 0.1$, whereas the dashed blue curve is when $b_s = 0.4$. (d) Evolution of the nonlinear JR state with the input condition taken from the dashed blue curve in (c). (e) Evolution of the nonlinear JR state with $\gamma = -1$ and $b_0 = 0.5$. (f) Evolution of the nonlinear JR state with the input condition taken from the red curve with round markers in (c). Other parameters: $\sigma_1 = -1$, $\sigma_2 = 1$, and $\kappa = 1$.

all nonlinear localized states that we have obtained are quite robust. This is also in agreement with the results obtained in the case of just Kerr nonlinearity in Ref. 27 (see Fig. 3 therein), which show that media with positive γ are able to form stable localized states for a wide range of peak amplitudes, whereas media with negative γ are only favorable for localized states with a low peak intensity.

Note also that one can make a localized state with a negative γ more stable by decreasing its initial peak amplitude as shown in Fig. 2(e) where all parameters are exactly the same as in Fig. 2(f) except for a lower initial peak amplitude b_0 [$b_0 = 0.5$ in Fig. 2(e), but $b_0 = 0.8$ in Fig. 2(f)]. Physically, the mechanism for stabilizing localized states in this case is similar to the one just mentioned above when b_s is increased. Indeed, as pointed out in Ref. 27 where localized states with just Kerr nonlinearity have been analyzed and mentioned just above, media with negative γ can only support localized states with low peak amplitudes. In other words, in self-defocusing media with Kerr nonlinearity (i.e., when $\gamma < 0$), localized states can be supported only in the case when the nonlinear term is small in

an absolute value. This is understandable because in the case of Kerr nonlinearity with $\gamma < 0$, the nonlinear term leads to the *defocusing*, i.e., broadening of the beams. That is why if $\gamma < 0$, we need to keep the nonlinear term small in an absolute value if we want to create a favorable condition for generating localized states. In the case of cubic–quintic nonlinearity with $\gamma < 0$, because b_s is always positive and $1 - b_s|b_n|^2 > 0$, one can decrease the influence of the nonlinear cubic–quintic term (last term) in Eq. (9) by two ways: either by decreasing the peak amplitude b_0 or by increasing the saturation parameter b_s. That is the reason why both these ways are able to stabilize localized states in the case of cubic–quintic nonlinearity as shown in Figs. 2(d) and 2(e).

It is worth emphasizing that profiles of localized states in interfaced BWAs with Kerr nonlinearity reported in Ref. 27 have a very interesting feature: their peak amplitude and transverse dimension can increase (or decrease) at the same time. Our results in this work confirm that this distinguishing feature of localized states in interfaced BWAs exists not only for Kerr nonlinearity, but also for
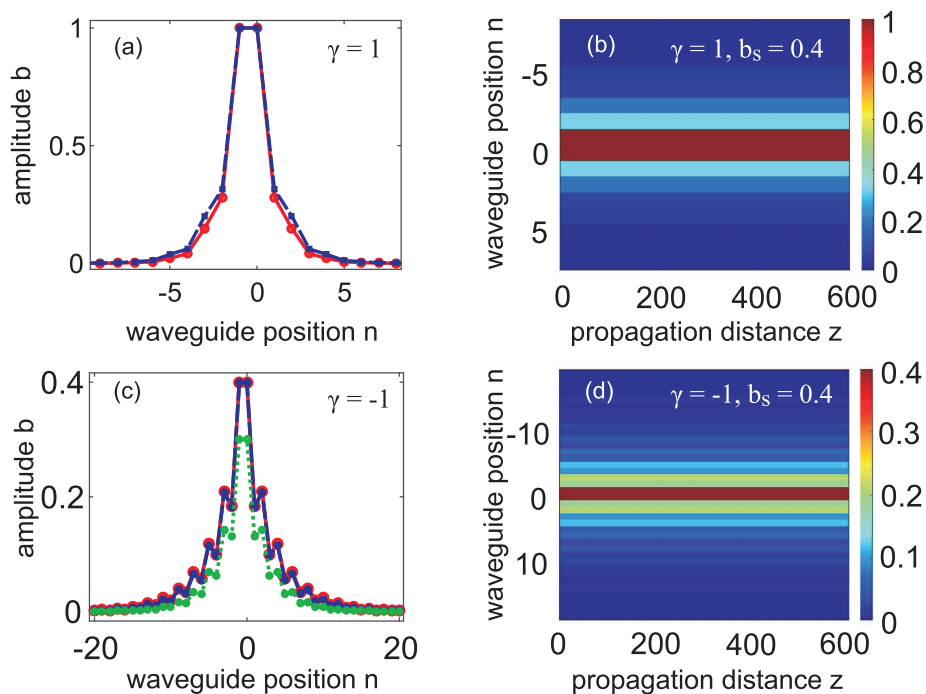
FIG. 3. Trivial localized states in interfaced BWAs with cubic–quintic non-linearity. (a) Amplitude profile b_n when $\gamma = 1$ and $b_0 = 1$: the red curve with round markers is obtained with $b_s = 0.1$, whereas the dashed blue curve is obtained with $b_s = 0.4$. (b) Evolution of the trivial state with the input condition taken from the dashed blue curve in (a). (c) Amplitude profiles when $\gamma = -1$: the red curve with round markers is obtained when $b_s = 0.1$ and $b_0 = 0.4$, the dashed blue curve is obtained when $b_s = 0.4$ and $b_0 = 0.4$, whereas the dotted green curve is obtained when $b_s = 0.4$ and $b_0 = 0.3$. (d) Evolution of the trivial state with the input condition taken from the dashed blue curve in (c). Other parameters: $\sigma_1 = 1$, $\sigma_2 = -1$, and $\kappa = 1$.

cubic–quintic nonlinearity. Indeed, in Fig. 2(a), the dashed blue curve and the dotted green curve of discrete JR states are obtained when all parameters are exactly the same except for the peak amplitude (and the eigenvalue detuning, obviously). We see that the dotted green curve with a lower peak amplitude is totally enveloped by the dashed blue curve with a higher peak amplitude. The same situations happen for the dashed blue curve and the dotted green curve of trivial states in Fig. 3(c). Meanwhile, for *many* other well-known localized structures and optical solitons found in bulk media, discrete solitons in a conventional WA,[4] and even discrete Dirac solitons in a periodic BWA (i.e., without the interface) found in Ref. 11, these two characteristic parameters always vary in an opposite manner: the peak increase will lead to the spatial narrowing of the beam (or the temporal shortening of the pulse) and vice versa. Note that, quite recently, it has been experimentally shown in Ref. 24 that in a waveguide array (possessing Kerr nonlinearity) with periodic variations along the waveguide axis, the degree of spatial localization of Floquet solitons in a topological bandgap first increases, then *decreases* after reaching its maximum as the input power increases (see Fig. 3 therein).

IV. DETUNINGS OF JACKIW–REBBI STATES AND TRIVIAL STATES WITH CUBIC–QUINTIC NONLINEARITY

Now, we study in detail the dependence of the localized state detunings on their peak amplitudes and other parameters. In Fig. 4(a), we present the relative detuning δ/δ_1 of discrete JR states as a function of the peak amplitude b_0 in the case of cubic–quintic nonlinearity with the saturation parameter $b_s = 0.1$. We get the

red curve having diamond markers in Fig. 4(a) when $\gamma = 1$, $\sigma_1 = -1$, and $\sigma_2 = 1$. Meanwhile, we get the green curve having round markers in Fig. 4(a) when $\gamma = -1, \sigma_1 = -1$, and $\sigma_2 = 1$ (i.e., when we only change the sign of γ). These two curves are practically symmetrical with the black horizontal axis (which shows the detuning δ_1 of the linear discrete JR states) serving as the symmetry line. Indeed, in Fig. 4(a), the dashed red curve (which is the artificial image of the red curve having diamond markers) coincides very well with the green curve having round markers. There is only one significant difference between these two curves: the one with positive γ can be drawn further for higher peak amplitude b_0, whereas the other one with negative γ stops at the maximum value $b_0 \simeq 0.85$, and we cannot find localized solutions for JR states with a higher value b_0 in this case. The symmetry of the two curves representing detunings of localized states in BWAs with just Kerr nonlinearity while switching the sign of γ and keeping all other parameters fixed has been explained in detail in Sec. 4 in Ref. 27. This explanation is also valid for localized states in interfaced BWAs of all other types of nonlinearity, including the cubic–quintic term as in this work. Indeed, like in Ref. 27 dealing with Kerr nonlinearity, we now introduce δ_l as the detuning of *linear* localized states; i.e., $\delta_l = \delta_1$ for linear JR states and $\delta_l = \delta_2$ for trivial states. In the case of γ, we use δ as the detuning of the nonlinear localized states possessing a peak amplitude b_0. Then, we change the sign of the nonlinear coefficient γ so that $\gamma \rightarrow -\gamma$. In that way, the new nonlinear localized states will have the detuning δ' instead of δ and the amplitude c_n instead of b_n. If the curve representing δ/δ_l and the curve representing δ'/δ_l are almost symmetrical with respect to the black horizontal axis in Fig. 4, the following relationship, $\delta/\delta_l \simeq 2 - \delta'/\delta_l$, must take place.
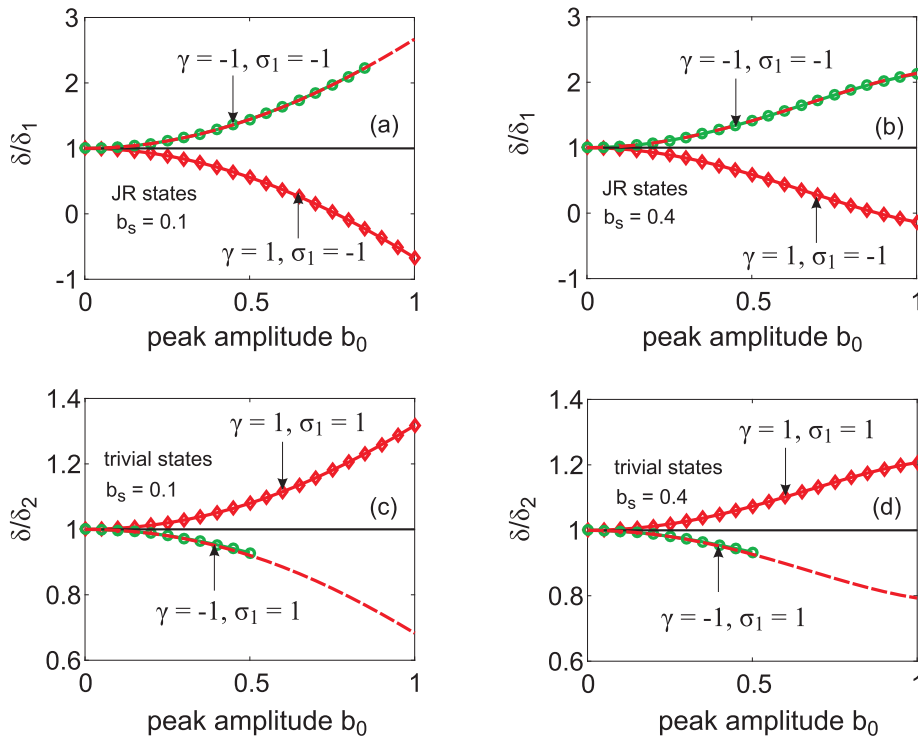
FIG. 4. Relative detuning of nonlinear localized states as functions of the peak amplitude b_0 in the case of cubic–quintic nonlinearity. (a) and (b) The curves are obtained for discrete JR states with the saturation parameter $b_s = 0.1$ in (a) and $b_s = 0.4$ in (b). (c) and (d) Exactly the same as in (a) and (b), respectively, but for trivial states. The dashed red curves in Fig. 4 are the artificial mirror images of the red curves having diamond markers with the black horizontal axis serving as the symmetry line. The coupling coefficient $\kappa = 1$, as usual. All other parameters are indicated for each curve therein.

Therefore, we need to have $\delta' \simeq 2\delta_l - \delta$. As a result, in the case of $-\gamma$, Eq. (9) will be now rewritten as follows:

$$-(2\delta_l - \delta)c_n \simeq -\kappa[c_{n+1} + c_{n-1}] + (-1)^n \sigma c_n$$
$$+ \gamma(1 - b_s|c_n|^2)|c_n|^2 c_n. \quad (10)$$

By adding Eq. (9) to (10), we obtain a new system of equations:

$$\delta(c_n - b_n) - 2\delta_l c_n \simeq -\kappa[(c_{n+1} + b_{n+1}) + (c_{n-1} + b_{n-1})]$$
$$+ (-1)^n \sigma(c_n + b_n) + \gamma(|c_n|^2 c_n - |b_n|^2 b_n)$$
$$+ \gamma b_s(|b_n|^4 b_n - |c_n|^4 c_n). \quad (11)$$

Now, if we keep the peak amplitudes $b_0 = c_0$ at small values and note that the condition $c_n \simeq b_n$ is always held true in this low-power regime, then all the nonlinear terms in Eq. (11) will practically vanish. As a result, from Eq. (11), we will have

$$-\delta_l c_n \simeq -\kappa[c_{n+1} + c_{n-1}] + (-1)^n \sigma c_n. \quad (12)$$

The system of Eq. (12) is always satisfied in the low-power regime because δ_l therein is the detuning of the *linear* localized states [see also Eq. (9) if $\gamma = 0$].

Therefore, in interfaced BWAs with cubic–quintic nonlinearity, we have proved that by fixing all parameters except for the sign of γ, we will also get two curves plotting relative detunings of nonlinear localized states, which are practically symmetrical with the axis (which shows the detuning of the corresponding *linear* localized states) serving as the symmetry line. This symmetry is satisfied very well when the peak amplitude of nonlinear localized states is

small, but the violation of this symmetry will be more and more significant if we increase the peak amplitude of nonlinear localized states.

It is interesting to note that the termination of the upper branch with $\gamma = -1$ in Fig. 4(a) for the JR state happens when its nonlinear detuning δ approaches the bottom edge of the gap; i.e., $\delta \to -\sigma_0$. Indeed, for parameters used in Fig. 4(a), we have the linear detuning of the gap JR state $\delta_1 = -0.4142$, which obviously lies inside the gap from -1 to 1. When the peak amplitude of the nonlinear JR states increases, the detuning of the upper branch approaches the bottom edge (-1) of the gap and stops at $\delta \simeq 2.227 * \delta_1 \simeq -0.9224$. Therefore, all the detunings (both linear and nonlinear, both for $\gamma = -1$ and $\gamma = 1$) of the JR states in Fig. 4(a) lie inside the gap from $-\sigma_0$ to σ_0. This is also true for the JR states in Fig. 4(b). Moreover, we want to emphasize that this interesting property is also true for JR states with Kerr nonlinearity analyzed in Ref. 27 [see Fig. 3(a) therein].

In Fig. 4(b), we plot the same quantities as in Fig. 4(a) with the only difference that now $b_s = 0.4$. One can see that the larger value of the saturation parameter b_s in Fig. 4(b) helps in developing the green curve having round markers further for higher values of the peak amplitude b_0. This fact is possible because if $\gamma < 0$, then the quintic term with b_s in Eq. (9) acts as the self-focusing nonlinearity, which helps in balancing the effect of the self-defocusing nonlinearity of the cubic term for higher peak amplitudes. Note that, as pointed out in Ref. 27 and mentioned above, the self-focusing nonlinearity is always more favorable to support high-intensity JR states than the self-defocusing nonlinearity.

In Figs. 4(c) and 4(d), we present the dependence of the relative detuning δ/δ_2 for nonlinear trivial states on the peak amplitude b_0. All parameters and curves in Figs. 4(c) and 4(d) are exactly similar to those in Figs. 4(a) and 4(b), respectively, with the only difference that Figs. 4(a) and 4(b) represent the case of nonlinear discrete JR states, whereas Figs. 4(c) and 4(d) represent the case of nonlinear trivial states [as a result, σ_1 must be negative in Figs. 4(a) and 4(b) but positive in Figs. 4(c) and 4(d)]. One can see from Figs. 4(c) and (d) that it is also possible to obtain trivial states with high peak amplitudes in the regime of cubic–quintic nonlinearity for the case of positive γ. However, with a negative γ, one can only generate trivial states with rather low peak amplitudes $b_0 \leq 0.5$ in Figs. 4(c) and 4(d). Note that one can get discrete JR states with higher peak amplitudes b_0 for a negative γ in Figs. 4(a) and 4(b). This situation is quite similar to the case of Kerr nonlinearity reported in Ref. 27. Note also that the larger value of the saturation parameter b_s in Fig. 4(d) does not help to generate trivial states with higher peak amplitudes [two green curves with round markers stop at $b_0 = 0.5$ in both Fig. 4(c) with $b_s = 0.1$ and Fig. 4(d) with $b_s = 0.4$]. We conjecture that this is because with a negative γ, nonlinear trivial states are much less transversally localized than nonlinear JR states. As a result, it is always more problematic to obtain the nonlinear localized trivial states with intense peak amplitudes when $\gamma = -1$.

V. CONCLUSIONS

In this work, we have systematically studied two types of localized states—the optical analogs of quantum relativistic Jackiw–Rebbi states and trivial localized states—in interfaced BWAs in the regime of cubic–quintic nonlinearity. We have shown that large values of the saturation nonlinearity parameter can help to generate and stabilize localized states of both types with high peak amplitudes, especially in the case of a negative coefficient for the cubic nonlinearity term. Like the profiles of localized states with just Kerr nonlinearity, those of localized states with cubic–quintic nonlinearity in interfaced BWAs possess an extraordinary feature that *many* other well-known localized nonlinear structures do not have. Specifically, both the peak amplitude and transverse dimension of these nonlinear localized states can increase (or decrease) simultaneously. We have also revealed that localized states with the positive sign of the coefficient for the cubic term can be formed with high peak amplitudes, whereas those with the negative sign can be formed only with a low peak amplitude. We have also demonstrated that if we only switch the sign of the coefficient for the cubic nonlinearity term and keep all other parameters unchanged, then we can get two curves representing the relative detunings of nonlinear localized states, which are practically symmetrical where the axis plotting the linear localized state detuning serves as the symmetry line. This general rule is applicable for all types of localized states with various kinds of nonlinearity in binary waveguide arrays.

DATA AVAILABILITY

The data that support the findings of this study are available from the corresponding author upon reasonable request.

REFERENCES

[1] D. N. Christodoulides, F. Lederer, and Y. Silberberg, Nature **424**, 817–823 (2003).
[2] A. L. Jones, J. Opt. Soc. Am. **55**, 261–269 (1965).
[3] D. N. Christodoulides and R. I. Joseph, Opt. Lett. **13**, 794–796 (1988).
[4] Y. S. Kivshar and G. P. Agrawal, *Optical Solitons: From Fibers to Photonic Crystals* (Academic Press, 2003).
[5] G. P. Agrawal, *Applications of Nonlinear Fiber Optics*, 2nd ed., Academic Press, 2008).
[6] Tr. X. Tran and F. Biancalana, Phys. Rev. Lett. **110**, 113903 (2013).
[7] U. Peschel, T. Pertsch, and F. Lederer, Opt. Lett. **23**, 1701–1703 (1998).
[8] M. Ghulinyan, C. J. Oton, Z. Gaburro, L. Pavesi, C. Toninelli, and D. S. Wiersma, Phys. Rev. Lett. **94**, 127401 (2005).
[9] F. Dreisow, M. Heinrich, R. Keil, A. Tünnermann, S. Nolte, S. Longhi, and A. Szameit, Phys. Rev. Lett. **105**, 143902 (2010).
[10] F. Dreisow, R. Keil, A. Tünnermann, S. Nolte, S. Longhi, and A. Szameit, Europhys. Lett. **97**, 10008–10013 (2012).
[11] Tr. X. Tran, S. Longhi, and F. Biancalana, Ann. Phys. **340**, 179–187 (2014).
[12] Tr. X. Tran, X. N. Nguyen, and D. C. Duong, J. Opt. Soc. Am. B **31**, 1132–1136 (2014).
[13] Tr. X. Tran and D. C. Duong, Ann. Phys. **361**, 501–508 (2015).
[14] Tr. X. Tran, X. N. Nguyen, and F. Biancalana, Phys. Rev. A **91**, 023814 (2015).
[15] Tr. X. Tran and D. C. Duong, Chaos **28**, 013112–013119 (2018).
[16] Tr. X. Tran, J. Opt. Soc. Am. B **36**, 2001–2006 (2019).
[17] Tr. X. Tran and F. Biancalana, Phys. Rev. A **96**, 013831 (2017).
[18] R. Jackiw and C. Rebbi, Phys. Rev. D **13**, 3398 (1976).
[19] R. B. Laughlin, Rev. Mod. Phys. **71**, 863–874 (1999).
[20] M. Z. Hasan and C. L. Kane, Rev. Mod. Phys. **82**, 3045–3067 (2010).
[21] N. Malkova, I. Hromada, X. Wang, G. Bryant, and Z. Chen, Opt. Lett. **34**, 1633–1635 (2009).
[22] M. C. Rechtsman, J. M. Zeuner, Y. Plotnik, Y. Lumer, D. Podolsky, F. Dreisow, S. Nolte, M. Segev, and A. Szameit, Nature **496**, 196–200 (2013).
[23] A. Blanco-Redondo, I. Andonegui, M. J. Collins, G. Harari, Y. Lumer, M. C. Rechtsman, B. J. Eggleton, and M. Segev, Phys. Rev. Lett. **116**, 163901 (2016).
[24] S. Mukherjee and M. C. Rechtsman, Science **368**, 856–859 (2020).
[25] Tr. X. Tran, J. Opt. Soc. Am. B **36**, 2559–2563 (2019).
[26] Tr. X. Tran and F. Biancalana, J. Light. Technol. **35**, 5092–5097 (2017).
[27] Tr. X. Tran, Hue M. Nguyen, and D. C. Duong, Phys. Rev. A **100**, 053849 (2019).
[28] N. N. Rosanov and Tr. X. Tran, Chaos **17**, 037114 (2007).
[29] *Dissipative Solitons*, edited by N. Akhmediev and A. Ankiewicz (Springer, New York, 2005).
[30] R. Carretero-González, J. D. Talley, C. Chong, and B. A. Malomed, Physica D **216**, 77–89 (2006).
[31] A. Maluckov, L. Hadžievski, and B. A. Malomed, Phys. Rev. E **76**, 046605 (2007).
[32] A. Maluckov, L. Hadžievski, and B. A. Malomed, Phys. Rev. E **77**, 036604 (2008).
[33] C. M. Cortés, R. A. Vicencio, and B. A. Malomed, Phys. Rev. E **88**, 052901 (2013).
[34] C. Chong, R. Carretero-González, B. A. Malomed, and P. G. Kevrekidis, Physica D **238**, 126–136 (2009).
[35] G. P. Agrawal, *Nonlinear Fiber Optics*, 5th ed. (Academic Press, 2013).
[36] S. Longhi, Opt. Lett. **35**, 235–237 (2010).
[37] T. Yefsah, A. T. Sommer, M. J. H. Ku, L. W. Cheuk, W. Ji, W. S. Bakr, and M. W. Zwierlein, Nature **499**, 426–430 (2013).
[38] D. G. Angelakis, P. Das, and C. Noh, Sci. Rep. **4**, 6110–6115 (2014).
[39] A. A. Sukhorukov and Y. S. Kivshar, Opt. Lett. **27**, 2112–2114 (2002).
[40] R. Morandotti, U. Peschel, J. S. Aitchison, H. S. Eisenberg, and Y. Silberberg, Phys. Rev. Lett. **83**, 4756 (1999).